Nuclear Physics A475 (1987) 579-597
North-Holland, Amsterdam

MICROSCOPIC THEORY OF PHOTON PRODUCTION IN PROTON-NUCLEUS AND NUCLEUS-NUCLEUS COLLISIONS*

T.S. BIRO[1], K. NIITA, A.L. DE PAOLI[2], W. BAUER, W. CASSING and U. MOSEL

Institut für Theoretische Physik, Universität Giessen 6300 Giessen, West Germany

Received 14 April 1987
(Revised 17 June 1987)

Abstract: The production of energetic photons in medium-energy proton and heavy-ion induced reactions is studied on the basis of incoherent nucleon-nucleon collisions. For this purpose we first evaluate covariantly the photon production from proton-neutron collisions in a vector (ω) and scalar meson (σ) exchange model with coupling constants given by the M2Y G-matrix in the nonrelativistic limit. We furthermore follow the proton-neutron collisional history by means of a phase-space simulation based on the Boltzmann-Uehling-Uhlenbeck approach for proton-nucleus and nucleus-nucleus collisions adding up incoherently the yields from each individual collision. The satisfactory agreement we obtain in comparison with experimental data allows to conclude that energetic photons predominantly arise from proton-neutron bremsstrahlung during the early stage of the collision.

1. Introduction

Experiments on energetic photon production in intermediate energy heavy-ion collisions show a significant yield of photons with energies above 50 MeV [refs. [1-8]] which had originally been proposed to originate from coherent nucleus-nucleus bremsstrahlung [9-11]). Meanwhile, there are indications against collective bremsstrahlung both from theoretical studies [12,13]) as well as experimental data [1-7]), since measured source velocities are those of the nucleon-nucleon center-of-mass [3,4,7]) and experimental angular distributions of energetic photons turn out to be rather isotropic in the nucleon-nucleon center-of-mass system. Furthermore, microscopic calculations [12]) without the deceleration-time parameters of the classical models tend to underpredict the experimental yield by more than one order of magnitude. The cooperative (statistical) model of Shyam and Knoll [14]) on the other hand systematically overpredicts the photon cross section by more than an order of magnitude [15]) and in the case of pions by roughly a factor of 5. In summary, there exists no compelling evidence for the presence of any cooperative effects so far.

* Supported by BMFT and GSI Darmstadt.

[1] On leave from the CRIP Budapest, Hungary.

[2] Supported by a fellowship of the Consejo Nacional de Investigaciones Cientificas y Technicas, Republica Argentina.

0375-9474/87/$03.50 © Elsevier Science Publishers B.V.
(North-Holland Physics Publishing Division)

Nucleon–nucleon bremsstrahlung is an alternative production mechanism [16]). Indeed it was found in the calculations of Ko *et al.* [17]) that neutron–proton bremsstrahlung was more important than coherent bremsstrahlung except for collisions of very heavy nuclei. Furthermore, neutron–proton (np) bremsstrahlung as evaluated for first chance np collisions within a quantum mechanical phase-space model [18]) gives overall agreement with the total cross-section of photons above 50 MeV. In the case of exclusive measurements the double differential cross sections can also be well understood within this approach [7]).

In ref. [19]) we have used the classical phase-space approach based on the Boltzmann–Uehling–Uhlenbeck equation [20–22]) in order to follow the time-development of those pn collisions which could produce an energetic photon. The results of these investigations rule out energetic photon emission from pn collisions in a nuclear fireball as proposed in refs. [16,23]) since photons are found to be produced in the very early stage of the heavy-ion reaction long before thermal equilibrium might be achieved.

In our earlier studies [18,19]) we used the hard scattering limit [24]) for the elementary process $pn \to pn\gamma$ which is not very satisfactory in the sense that it corresponds to a nonrelativistic soft photon limit or a $1/\omega$ expansion in the cross-section. We thus improve this description in sect. 2 by evaluating in a covariant way the radiative corrections to the nucleon–nucleon vertices involving vector meson (ω) and scalar meson (σ) exchange in close analogy to studies performed in the later sixties [25]) and early seventies [26,27]). We restrict ourselves to proton–neutron vertices since proton–proton bremsstrahlung was found experimentally to be more than an order of magnitude smaller than $pn \to pn\gamma$ [ref. [28])].

Sect. 3 contains a detailed description of proton–nucleus and nucleus–nucleus reaction dynamics within the BUU limit [19–22]) while sect. 4 shows the results for double differential photon yields. A comparison with available experimental data as well as with the hard scattering limit for $pn \to pn\gamma$ is included. In sect. 5 a detailed analysis of initial and final phase-space distributions as well as source velocity distributions for $^{12}C + ^{12}C$ and $^{12}C + ^{40}Ca$ at 40 MeV/u is performed. Final conclusions and open problems are addressed in sect. 6.

2. Covariant calculation of γ-production in pn collisions

According to experimental and theoretical studies the photon production in nucleon–nucleon reactions is dominated by the $pn \to pn\gamma$ process since $pp \to pp\gamma$ is suppressed by about an order of magnitude [28]) due to destructive interference of the radiation from each of the two protons. Because of the rather involved 5-body kinematics in such reactions there are not enough experimental data to cover the complete range of γ-energies and -angles for all initial and final nucleon momenta. For the purpose of modelling γ-production in heavy ion collisions we, therefore, cannot use the "free" $pn \to pn\gamma$ cross sections as "experimental" input.

Besides this "practical" problem there is a more physical motivation to use model calculations for describing the $pn \to pn\gamma$ process, namely that "free" elementary cross sections may be considerably different from in-medium cross sections [29,30].

In our earlier studies [18,19] we used the nonrelativistic long wavelength ($1/\omega$) expansion [24] for the elementary process $pn \to pn\gamma$, i.e.

$$\frac{d^2\sigma}{d\omega\, d\Omega_\gamma} = \frac{e^2}{4\pi} \frac{\pi R^2}{4\pi^2} \frac{\beta^2}{\omega} [\sin^2 \theta_\gamma + \tfrac{2}{3}] , \tag{2.1}$$

where β denotes the velocity of the nucleons in the nucleon-nucleon c.m. frame and πR^2 the angle integrated elastic pn cross section.

This cross section is peaked at 90° in the pn center-of-mass system. The 5:2 ratio of $\sigma(90°):\sigma(0°)$ can be decreased by assuming a forward (backward) peaked elastic pn cross section, which is justified for relative energies above 100 MeV [ref. [31]]. The change, however, is rather minor; the ratio stays between 5:2 and 2:1. The experimental results - at least from heavy-ion collisions - show a much flatter angular distribution [1-3]. Such a flatness could be due to a relativistic effect that leads to a forward peaking of the bremsstrahlung distributions [24]. A summation over all pn and np collisions will then yield a flatter angular distribution in the case of heavy-ion reactions.

In order to remedy the former deficiences we employ here a relativistic covariant meson-exchange model to describe the elementary γ-production cross section. In this way we also get rid of the long wavelength approximation as in ref. [23].

Utilizing a fit for the in-medium nucleon-nucleon interaction in terms of two Yukawa potentials by Bertsch *et al.* [32] we consider a relativistic extension in terms of one-boson exchange of scalar- and vector-type with masses $m_s = 492.5$ MeV $= 1/0.4\ \mathrm{fm}^{-1}$, $m_v = 788$ MeV $= 1/0.25\ \mathrm{fm}^{-1}$ and weight factors $g_s^2/4\pi = 4.356$, $g_v^2/4\pi = 11.49$, respectively. It is interesting to note that the masses of the exchanged mesons are surprisingly close to those used in the relativistic mean-field theory of nuclear structure [29].

For the transition matrix of the $pn \to pn\gamma$ process we have contributions from four different amplitudes according to photon radiation before or after the pn interaction and scalar or vector meson exchange. The antisymmetrization of the fermion final states brings an extra factor of 2, so altogether we deal with $8^2 = 64$ terms in the cross section formula (the corresponding amplitudes are depicted in fig. 1 in terms of Feynman diagrams).

The square of the transition matrix reads:

$$|\tau_{fi}|^2 = \frac{1}{16} \sum_{\text{spins}} |\tau_1^s + \tau_1^v + \tau_3^s + \tau_3^v - \tau_{1,Ex}^s - \tau_{1,Ex}^v - \tau_{4,Ex}^s - \tau_{4,Ex}^v|^2 , \tag{2.2}$$

where

$$\tau_1^{s,v} = \frac{e G_{s,v}(p_3 - p_1)}{-2(p_1 \cdot k)} [\bar{u}_4 u_2][\bar{u}_3 \Gamma^{1-k} \gamma_\mu u_1] \tag{2.3}$$

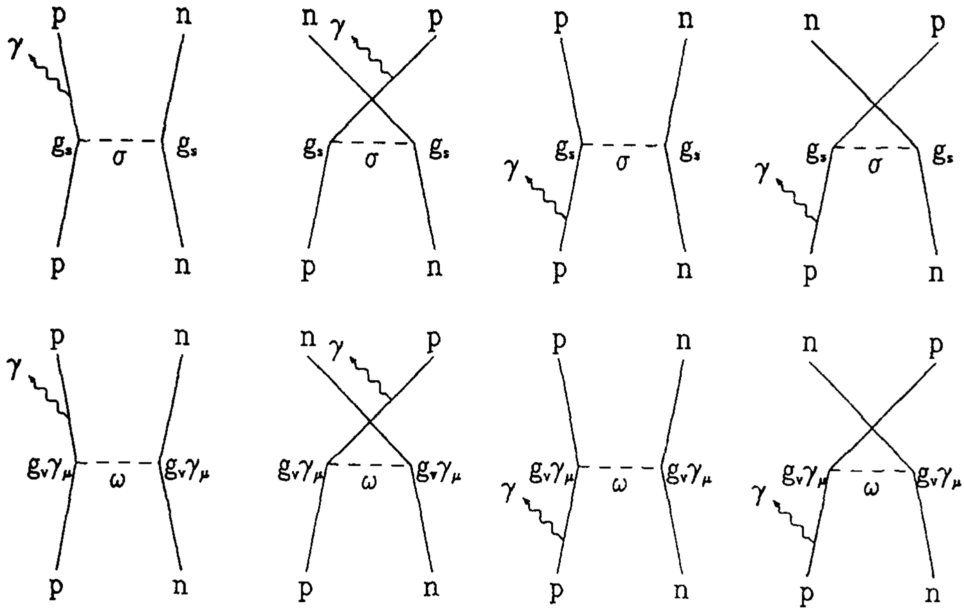

Fig. 1. The Feynman graphs corresponding to radiative corrections of scalar- and vector meson exchange in the process $pn \to pn\gamma$.

describes the pre-collision amplitude and

$$\tau_3^{s,v} = \frac{eG_{s,v}(p_3 - p_1)}{2(p_3 \cdot k)}(\bar{u}_4 u_2)(\bar{u}_3 \gamma_\mu \Gamma^{3+k} u_1) \tag{2.4}$$

the post-collision amplitude.

The propagators G_s and G_v in (2.3) and (2.4) are given by:

$$G_s(p) = \frac{g_s^2}{p^2 - m_s^2}, \tag{2.5}$$

$$G_v(p) = -\gamma_\alpha \frac{g_v^2}{p^2 - m_v^2} \gamma^\alpha, \tag{2.6}$$

where γ_α denote the four Dirac matrices.

The exchange amplitudes can easily be derived from the corresponding direct ones by interchanging the indices 3 and 4. The indices 1 to 4 denote the nucleons in the order $pn \to pn\gamma$ ([1][2]$\to$[3][4]γ) or for the exchange contributions $pn \to np\gamma$ ([1][2]$\to$[4][3]γ), respectively. $u_i(\bar{u}_i)$ is a corresponding Dirac spinor attached to a fermion initial (final) state and $\Gamma^{i\pm k}$ stands for:

$$\Gamma^{i\pm k} = [\gamma^\mu (p_\mu^i \pm k) + m]. \tag{2.7}$$

Due to the square of the absolute value in (2.2) pairs of spinors (lying on the same fermion line) are replaced by the projection

$$\bar{u}_i u_i \to \Gamma^i / 2m. \tag{2.8}$$

The summation (average) over final fermion states includes a trace of long products of a number of Dirac matrices (γ_α). These expressions are quite lengthy and are obtained by means of the algebraic manipulation software REDUCE 3.2.

Once the square of the transition matrix is expressed by the four-momenta of in- and outgoing fermions (i.e. the photon four-momenta can be eliminated through energy- and momentum-conservation) one can obtain the differential γ-production cross section by multiplying the appropriate kinematical and phase-space factors [33]):

$$\frac{d\sigma}{d\tilde{k}}=\frac{m^2}{[(p_1\cdot p_2)^2-m^4]^{1/2}}|\tau_{fi}|^2\, d\tilde{p}_3\, d\tilde{p}_4(2\pi)^4\delta^4(P_f-P_i)\,, \tag{2.9}$$

where

$$d\tilde{p}_i=\frac{d^3p_i}{(2\pi)^3}\frac{m}{\sqrt{m^2+p_i^2}} \quad \text{for nucleons}\,, \tag{2.10}$$

$$d\tilde{k}=\frac{d^3k}{(2\pi)^3}\frac{1}{2\omega} \quad \text{for photons,} \tag{2.11}$$

and $P_i=p_1+p_2$, $P_f=p_3+p_4+k$ denote the initial and final total four-momenta, respectively.

The resulting double differential photon cross section $d\sigma_\gamma/d\omega_\gamma\, d\Omega_\gamma$ calculated with one-boson (scalar+vector) Feynman graphs and free nucleon masses (middle part of fig. 2) shows a characteristically flatter angular distribution than the "semi-classical" $1/\omega$ expansion (l.h.s. of fig. 2), especially for high (near-threshold) photon

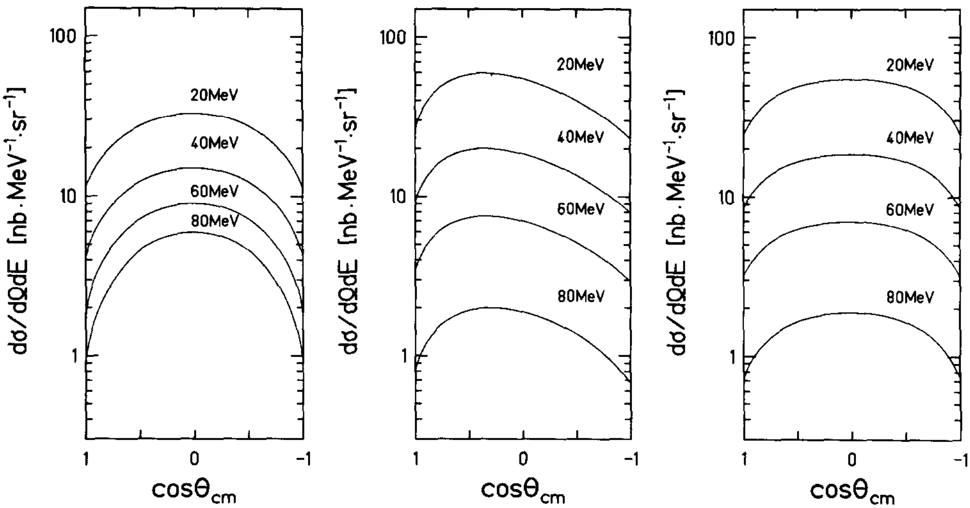

Fig. 2. Comparison of the double differential photon cross section from 200 MeV $pn \to pn\gamma$ in the semiclassical ($1/\omega$) limit (l.h.s.) and the relativistic OBE approximation (middle) for the various photon energies indicated in the figure. The photon angular distribution for the relativistic OBE approach symmetrized with respect to pn and np collisions is shown in addition (r.h.s.).

energies in case of p+n at 200 MeV. Most of this flattening is due to a relativistic effect; even in the long wavelength approximation the dipole-bremsstrahlung is forward peaked [24]. By symmetrizing the cross section with respect to pn and np collisions we obtain an even flatter angular distribution (r.h.s. of fig. 2). We note in passing that in the relativistic case (2.9) the semiclassical $1/\omega$ expansion after integration over $d\Omega_\gamma$ holds approximately for photon energies below 10 MeV. This energy regime, however, is of no interest in the context of the present study.

Summarizing the present section we have calculated the exclusive $pn \to pn\gamma$ cross section for all possible final states assuming free on-shell nucleons before and after γ-radiation. The underlying $pn \to pn$ interaction is simulated by a relativistic extension of the M2Y (G-matrix) potential fitted to low energy nuclear properties. A further extension of the model including radiation from pion exchange on the basis of the M3Y interaction yields almost identical results for $pn \to pn\gamma$ since the amplitude for pseudo-scalar pion exchange in the nuclear medium is small compared to scalar- and vector-meson exchange [32].

3. Heavy-ion reaction dynamics

After the evaluation of the elementary production cross section for high energy photons, we now need a model for the heavy-ion reaction dynamics to obtain information on the number of pn collisions during the heavy-ion collision and the momentum distribution of protons and neutrons.

In this context Nakayama and Bertsch [13] have used infinite nuclear matter Fermi-spheres to approximate the momentum distributions while in ref. [18] we used a phase-space distribution based on TDHF dynamics, but had to assume *ad hoc* that the photons were produced by first chance pn collisions only.

It is therefore desirable to use a transport theory for heavy-ion reactions which keeps track of the np collisional time-evolution. The only workable transport theory for heavy ion reactions in three dimensions at present is based on the Boltzmann-Uehling-Uhlenbeck equation [19-22]:

$$\frac{\partial f_1}{\partial t} - \nabla_p f_1 \cdot \nabla_r U + \nabla_r f_1 \cdot \frac{\boldsymbol{p}_1}{m} = \frac{4}{(2\pi)^3} \int d^3p_2\, d^3p_3\, d\Omega\, v_{12} \frac{d\sigma}{d\Omega} \delta_3(\boldsymbol{p}_1 + \boldsymbol{p}_2 - \boldsymbol{p}_3 - \boldsymbol{p}_4)$$
$$\times [f_3 f_4(1-f_1)(1-f_2) - f_1 f_2 (1-f_3)(1-f_4)] \qquad (3.1)$$

for the time evolution of the phase-space density $f_i = f(\boldsymbol{r}_i, \boldsymbol{p}_i, t)$.

In this equation v_{12} is the relative velocity of the two incoming nucleons in a NN collision while $d\sigma/d\Omega$ denotes the in-medium NN cross section and U is the mean-field potential. It would be desirable to derive U and $d\sigma/d\Omega$ from the same nucleon-nucleon interaction; however, at the present level of BUU approaches one chooses an easier way for describing nucleon-nucleon collisions in analogy to cascade models [34]. In the present calculation we use $d\sigma/d\Omega = \sigma_{tot}/4\pi$ for the nucleon-nucleon cross section with σ_{tot} determined from σ and ω exchange (cf. sect. 2) via the optical theorem. This yields an energy dependent nucleon-nucleon cross section which is very close to the values used in cascade simulations [34]) but as a function of the nucleon-nucleon c.m. energy lowered by about 15% to 50%. The latter fact is not surprising since the M2Y potential represents a fit to a G-matrix which includes virtual in-medium interactions and Pauli blocking for intermediate states which results in a reduction of the free nucleon-nucleon interaction. In addition the Pauli blocking for the final states is taken into account via the factor $(1-f(\boldsymbol{r}_i, \boldsymbol{p}_i; t))$ in the collision term.

Independently, the mean field potential U is obtained from a density-dependent Skyrme parametrization,

$$U(\rho(\boldsymbol{r})) = A\frac{\rho(\boldsymbol{r})}{\rho_0} + B\left(\frac{\rho(\boldsymbol{r})}{\rho_0}\right)^{\tau}, \tag{3.2}$$

where the three coefficients A, B, and τ are determined by demanding saturation at normal nuclear matter density, the right nuclear matter binding energy, and a certain nuclear compressibility. We choose:

$$\begin{aligned} A &= -218\ \mathrm{MeV}, \\ B &= 164\ \mathrm{MeV}, \\ \tau &= \tfrac{4}{3}. \end{aligned} \tag{3.3}$$

The corresponding equation of state in the one-body limit is:

$$\frac{E_\mathrm{B}}{A} = \tfrac{3}{5}\varepsilon_\mathrm{F}\left(\frac{\rho}{\rho_0}\right)^{2/3} - 109\ \mathrm{MeV}\frac{\rho}{\rho_0} + 70.3\ \mathrm{MeV}\left(\frac{\rho}{\rho_0}\right)^{4/3}, \tag{3.4}$$

where $\varepsilon_\mathrm{F} = 38.5$ MeV is the Fermi energy. It yields a nuclear matter binding energy $(E_\mathrm{B}/A)(\rho_0) = -15.75$ MeV, saturates at $\rho = \rho_0 = 0.17\ \mathrm{fm}^{-3}$ and results in a nuclear compressibility of $K = 235$ MeV.

Eq. (3.1) is solved within the test particle method [19,22]) using 100 test particles per nucleon. The initial conditions for target and projectile are individually provided by a Thomas-Fermi phase-space distribution

$$f(\boldsymbol{r}, \boldsymbol{p}, t=0) = \theta\left(p_\mathrm{F}\left(\frac{\rho(\boldsymbol{r})}{\rho_0}\right)^{1/3} - |\boldsymbol{p}|\right), \tag{3.5}$$

which are then shifted and boosted according to the beam energy and impact parameter desired.

Due to the relatively small contribution of the process $\mathrm{pn} \to \mathrm{pn}\gamma$ to the total nucleon-nucleon cross section, it is possible to calculate the photon production perturbatively. In this way we do not couple the emission of the photon back to the nucleonic motion. One should note, however, that it would not be possible to extract photon-photon or photon-nucleon correlations within the present treatment.

We obtain the number of emitted photons $N(b)$ as a function of the impact parameter b by summing (integrating) the differential photon emission probability $(d^2\sigma/dE'_\gamma\, d\Omega'_\gamma)/\sigma_{tot}$ (cf. sect. 2) over all proton-neutron collisions and taking Pauli blocking in the final state phase space of the two nucleons into account:

$$\frac{d^2N(b)}{dE_\gamma\, d\Omega_\gamma} = \sum_{\text{pn coll}} \int \frac{d\Omega}{4\pi} \frac{E_\gamma}{E'_\gamma} \left(\frac{d^2\sigma}{dE'_\gamma\, d\Omega'_\gamma} / \sigma_{tot} \right) [1 - f(\boldsymbol{r}, \boldsymbol{p}_3, t)][1 - f(\boldsymbol{r}, \boldsymbol{p}_4, t)] \,. \tag{3.6}$$

In this equation $\boldsymbol{r}$ and t indicate the space-time coordinates of each collision. The primes denote quantities in the individual np c.m. system which have to be transformed into the laboratory frame or the midrapidity frame, respectively. Ω finally denotes the solid angle of the relative momentum $\boldsymbol{p}_3 - \boldsymbol{p}_4$ which is not fixed by energy and momentum conservation and is chosen here randomly. The integration over $d\Omega/4\pi$ is then performed by an average over many such choices.

To obtain the double differential photon cross section for the nucleus-nucleus reaction, we finally have to integrate over impact parameter:

$$\frac{d^2\sigma}{dE_\gamma\, d\Omega_\gamma} = \int d^2b \frac{d^2N(b)}{dE_\gamma\, d\Omega_\gamma} \,. \tag{3.7}$$

The yields obtained from eq. (3.7) can be directly compared to inclusive experimental data without introducing adjustable parameters.

4. Comparison with experiment

4.1. PROTON-NUCLEUS COLLISIONS

First we compare our results to proton-nucleus data. In the case of a proton-nucleus reaction the incoming proton has fixed momentum given by the beam energy. The neutron has a momentum distribution and a spatial distribution given by the ground state configuration of the nucleus. Since the momentum distribution of the nucleons will not get distorted very much during the course of the proton-nucleus reaction, the proton-nucleus data serve as a useful check of the validity of the elementary photon production cross section.

In fig. 3 we compare the results of our calculation for 140 MeV proton-nucleus collisions to the data of Edgington and Rose [35]) for deuterium, aluminum, and carbon targets. The solid lines represent the results of a calculation using the relativistic elementary cross section (2.9) while the dashed lines show the results for the semiclassical one (2.1). For the case of deuterium we assumed a broad spatial distribution of neutrons according to the experimental radius of the deuterium.

The results of our calculation using the relativistic elementary cross section show excellent agreement with the experimental data for p+C and p+Al, while the spectra obtained with the semiclassical elementary cross section are slightly flatter than the experimental ones. Therefore, the relativistic correction of the elementary

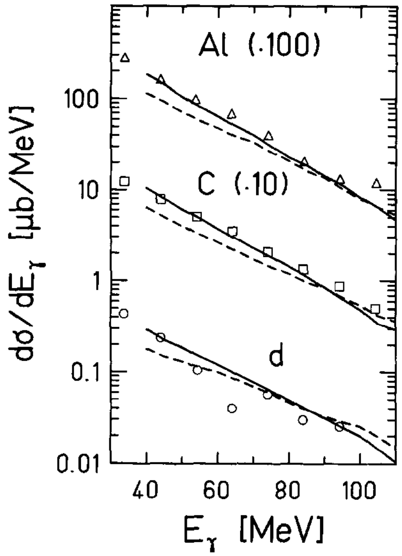

Fig. 3. Photon cross section $d\sigma/dE_\gamma$ for the reaction 140 MeV proton + nucleus. The solid lines are the results of our calculation with the relativistic elementary cross section and the dashed lines with the semiclassical elementary cross section. The data are taken from ref. [35]).

production cross section, which becomes more important near the threshold of the high energy photons, is necessary to explain the high energy photon spectra.

This can be seen more clearly in the angular distribution of energetic photons. Therefore, in fig. 4 we plot the differential cross section for photons with an energy above 40 MeV in the laboratory system for 140 MeV p + ^{12}C. This figure clearly shows that the relativistic correction of the elementary photon production cross section is essential to reproduce the angular distribution of energetic photons [35]). We conclude that the elementary cross section (2.9) evaluated in sect. 2 is sufficiently accurate to describe the photon production from incoherent proton–neutron collisions in the nuclear medium.

4.2. NUCLEUS-NUCLEUS COLLISIONS

We compare the results of our calculation within BUU dynamics to experimental data measured by Grosse *et al.* [1]) and Stevenson *et al* [3]). In fig. 5 we show the double differential cross section for photons emitted at an angle $\theta = 90°$ with respect to the beam axis. The three lower curves represent the results from N + C collisions at 40 (squares), 30 (triangles), and 20 (diamonds) MeV/nucleon beam energy [3]). The upper curve shows the results of a $^{12}C + ^{12}C$ collision at 84 MeV/nucleon beam energy (circles) [1]). The solid lines and the dashed lines are the results of our calculation with the same assignment as in fig. 3, respectively.

The results of the relativistic elementary cross section (solid lines) are in excellent agreement with the N + C data of Stevenson *et al.* More precisely, the beam energy

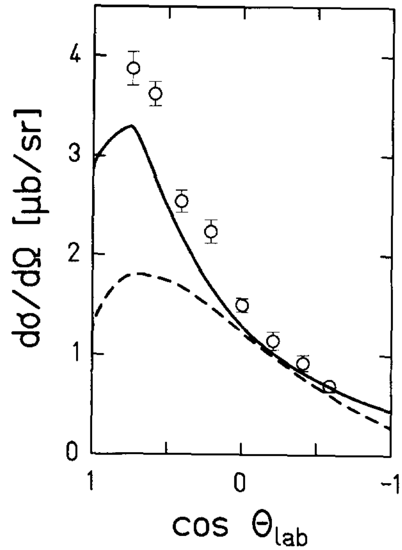

Fig. 4. Comparison of our calculation to photon angular distributions for the reaction 140 MeV p + ^{12}C. The solid lines and the dashed lines denote the same as in fig. 3. The data are taken from ref. [35]).

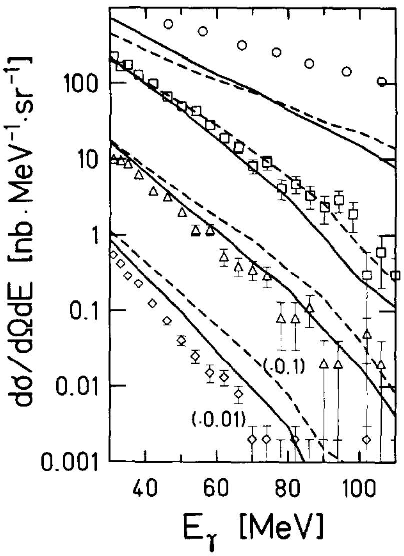

Fig. 5. Photon energy spectra from heavy-ion collisions. The solid lines and the dashed lines are the results of our calculations and denote the same as in fig. 3. The symbols represent the experimental data taken from refs. [1,3]). The emission angle of the photon is always 90° with respect to the beam axis. Circles: 84 MeV/u ^{12}C + ^{12}C; squares: 40 MeV/u ^{14}N + ^{12}C; triangles: 30 MeV/u ^{14}N + ^{12}C; diamonds: 20 MeV/u ^{14}N + ^{12}C.

dependence for the relativistic elementary cross section is more consistent with the N + C data than the results of the semiclassical one (dashed lines). Since the threshold of high energy photons decreases for the lower bombarding energy, the low frequency approximation of the semiclassical formula becomes worse with decreasing beam energy. This is why the deviation between the results of the calculation using the semiclassical cross section and the experimental data increases with decreasing beam energy.

On the other hand, we underpredict the 84 MeV/u C+C data of Grosse *et al.* [1]) as well as those at 74 and 60 MeV/u with both elementary photon production cross sections. For all beam energies our calculations are by a factor 2.5 to 3.5 lower than the data for high energy photons in the energy range between 50 and 100 MeV. This situation does not change if we use the relativistic formula for the elementary photon production cross section. We speculate that the data of Stevenson *et al.* and Grosse *et al.* are not fully compatible with each other.

Next we compare the calculated angular distribution of high energy photons to experimental data from Stevenson *et al.* and Grosse *et al.* In fig. 6 the double differential cross sections for photon energies of 40 MeV (circles), 60 MeV (diamonds), and 80 MeV (squares) are shown in the laboratory system for the $^{14}N+{}^{12}C$ collision at a beam energy of 40 MeV/u. The present results of the semiclassical elementary cross section (dashed lines) are slightly different from the results of our previous study [19]) especially at forward angles for the higher photon energies. This is due to the use of relativistic kinematics in the determination of the final

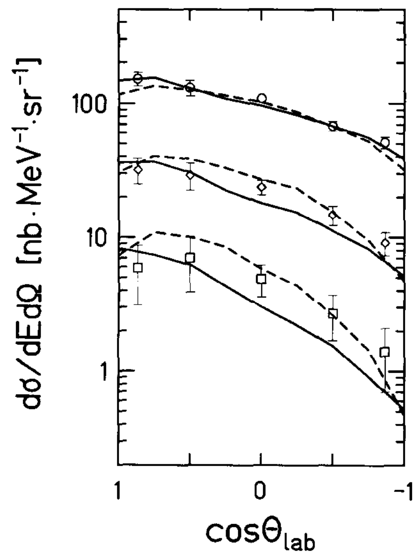

Fig. 6. Comparison of our calculation to the photon angular distributions measured by Stevenson *et al.* [3]) for a 40 MeV/u $^{14}N+{}^{12}C$ collision in the laboratory frame and photon energies of 40 (circles), 60 (diamonds), and 80 (squares) MeV. The solid lines and the dashed lines denote the same as in fig. 3.

momenta of proton and neutron, which had not been treated fully consistently in ref. [19]).

Both results of the different elementary cross section show very good agreement with the experimental angular distributions. With increasing photon energy, however, the differences between the calculations using the relativistic elementary cross section (solid lines) and the ones with the semiclassical expression (dashed lines) increase slightly. This difference is more visible in the angular distributions in the midrapidity frame. In fig. 7 we plot the experimental data of Grosse *et al.* for the differential cross section for photons with an energy between 50 and 100 MeV. The diamonds correspond to $E_{beam} = 84$ MeV/u, the squares to 74 MeV/u, and the circles to 60 MeV/u. Our results are shown by the solid and dashed lines, respectively, as in fig. 6. As mentioned before, our results usually underpredict the data of Grosse *et al.* To make the comparison of the angular distributions easier we therefore have scaled up all our results in fig. 7 by a factor 2.5.

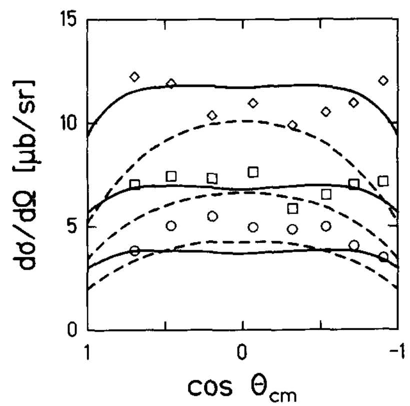

Fig. 7. Comparison of our calculations to the photon angular distribution measured by Grosse *et al.* [1]) for photons of energy between 50 and 100 MeV in the center-of-mass frame and beam energies of 84 (diamonds), 74 (squares), and 60 (circles) MeV/u. Our calculations (solid lines and dashed lines) have been uniformly scaled up by a factor of 2.5 to facilitate the comparison.

The angular distribution of the semiclassical elementary cross section is essentially of dipole shape. Though this shape is smeared out due to the Fermi motion of the colliding proton-neutron pair in the heavy-ion collision, the angular distributions obtained by using the semiclassical elementary cross section (dashed lines) still have a peak at 90°. This dipole-like shape gets more pronounced with increasing beam energy. However, the angular distributions of the experimental data are rather flat and show the opposite trend with increasing beam energy. On the other hand, the results of the relativistic elementary cross section are very close to isotropy and follow the experimental angular distribution quite well within the experimental error bars which we did not include in fig. 7 and which are typically 2 μb/sr for the 84 MeV/u data.

4.3. SCALING BEHAVIOUR OF ENERGETIC PHOTON YIELDS

The inclusive yield of energetic photons above 50 MeV as a function of the mass of projectile and target for fixed beam energy is expected to provide information on the collectivity of the production process [4,8]).

In order to get a closer idea of the scaling behaviour in our present treatment we have calculated the inclusive yield of energetic photons for collisions of symmetric systems ranging from mass 12 to mass 70 for a lab energy of 40 MeV/u. The shape of the spectra as well as the photon angular distribution are found not to change within the numerical uncertainties as a function of mass number. When performing cuts at different photon energies from 50 MeV to 100 MeV and dividing by the respective yield for $^{12}C + ^{12}C$ at the same energy we obtain a range of values for fixed mass which is shown in terms of the vertical lines in fig. 8. The result is compatible with $(A_1 \cdot A_2)^x$ with $x = 0.92$ which is indicated by the straight line in the double logarithmic plot. The fact that $x > \frac{2}{3}$ reflects a volume-contribution to the photon production; energetic photons are predominantly produced over a distance of about 3 fm in the target/projectile nucleus.

Performing a similar analysis for the experimental data from ref. [8]) we obtain $x = 0.87 \pm 0.05$ well in line with our calculations. One should note that contributions from collective bremsstrahlung, which might not be neglected for very heavy systems [17]), would yield a higher value of x in the region of heavy nuclei than for light

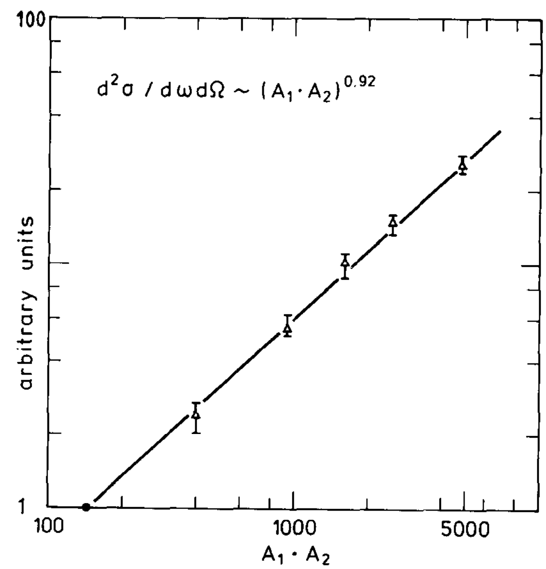

Fig. 8. Scaling behaviour of energetic photon yields with mass number of projectile and target $(A_1 \cdot A_2)$ for nucleus-nucleus collisions at 40 MeV/u. The straight line represents a fit to the calculated values as described in the text. The vertical bars give the cross section for various γ-energies between 50 and 100 MeV.

nuclei. Experimental data, however, show a slightly decreasing scaling exponent [8]) for heavy systems.

5. Phase-space analysis of energetic photon production

In a previous paper [19]) we have shown that the production of energetic γ-rays in nucleus-nucleus collisions by incoherent pn bremsstrahlung is limited to the very early phase of the reaction and restricted to the overlap regime of the colliding nuclei in coordinate space. In this section we are now interested in the dynamical origin of these photons in momentum space.

We consider a schematic np collision in momentum space producing a photon with momentum $\boldsymbol{k}_\gamma$ and energy $E_\gamma = \hbar c k_\gamma$ (fig. 9). The momenta of the colliding nucleons are denoted by $\boldsymbol{k}_1$ and $\boldsymbol{k}_2$, respectively, while their final momenta $\boldsymbol{k}_3$ and $\boldsymbol{k}_4$ are determined by momentum and energy conservation (cf. sect. 3). A photon with energy E_γ is then produced in the angular range $\mathrm{d}\Omega$ (with respect to the np c.m.s. and np axis) with the elementary probability $(\mathrm{d}^2\sigma_\gamma/\mathrm{d}E_\gamma\,\mathrm{d}\Omega)/\sigma_{\mathrm{tot}}$, where σ_{tot} denotes the total angle integrated nucleon-nucleon cross section for a relative momentum $|\boldsymbol{k}_1 - \boldsymbol{k}_2|$, multiplied by the probability that the phase-space cells around $\boldsymbol{k}_3$ and $\boldsymbol{k}_4$ are not occupied. Thus the relative probability for γ-production in the pn collision i, taking place at $t = t_i$ and $\boldsymbol{r} = \boldsymbol{r}_i$ in a fixed frame of reference, is given by

$$W_i(\boldsymbol{k}_1, \boldsymbol{k}_2; \boldsymbol{k}_\gamma) = \sigma_{\mathrm{tot}}^{-1}(|\boldsymbol{k}_1 - \boldsymbol{k}_2|)\frac{E_\gamma}{E'_\gamma}\frac{\mathrm{d}^2\sigma}{\mathrm{d}E'_\gamma\,\mathrm{d}\Omega'_\gamma}[1 - f(\boldsymbol{r}_i, \boldsymbol{k}_3; t_i)][1 - f(\boldsymbol{r}_i, \boldsymbol{k}_4; t_i)]\,, \quad (5.1)$$

where $(t_i, \boldsymbol{r}_i)$ as well as $f(\boldsymbol{r}_i, \boldsymbol{k}_3; t_i)$ are evaluated from BUU dynamics (cf. sect. 3). Here γ-energy and γ-angle are properly Lorentz-transformed from the nucleon-nucleon c.m. system to the laboratory frame.

The first question we address is related to the area in momentum space which contributes to the production of a photon with energy $E_\gamma = 100$ MeV under 90° in the laboratory frame with respect to the beam ($z-$) axis. The answer to this question

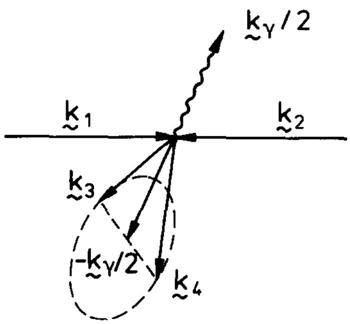

Fig. 9. Illustration of pn → pnγ kinematics in momentum space. The momenta of the colliding nucleons are denoted by $\boldsymbol{k}_1$ and $\boldsymbol{k}_2$, the photon momentum by $\boldsymbol{k}_\gamma$, and the final nucleon momenta by $\boldsymbol{k}_3$ and $\boldsymbol{k}_4$, respectively.

can be obtained by summing W_i over all np collisions

$$R(\boldsymbol{k}_1)=\sum_i \sum_{k_2} W_i(\boldsymbol{k}_1, \boldsymbol{k}_2; k_\gamma), \tag{5.2}$$

where we integrate also over $\boldsymbol{k}_2$ in order to reduce the number of degrees of freedom in $R(\boldsymbol{k}_1)$. Since $\boldsymbol{k}_1$ and $\boldsymbol{k}_2$ can be exchanged no information is lost in this integration.

The result for $R(k_x; k_y=0, k_z)$ is shown in fig. 10 in terms of a cluster plot for a central collision of $^{12}C+{}^{12}C$ at 40 MeV/u. We also display the phase-space distribution in the infinite nuclear matter limit given by two nonintersecting Fermi spheres shifted by $k_r \approx 1.4\,\mathrm{fm}^{-1}$ in beam direction according to the bombarding energy. It is clearly seen that a 100 MeV photon is predominantly produced by nucleons which come from the endcaps in z-direction of the elongated momentum distribution. Due to successive nucleon–nucleon collisions these energetic nucleons are available only in the initial phase of the heavy-ion reaction.

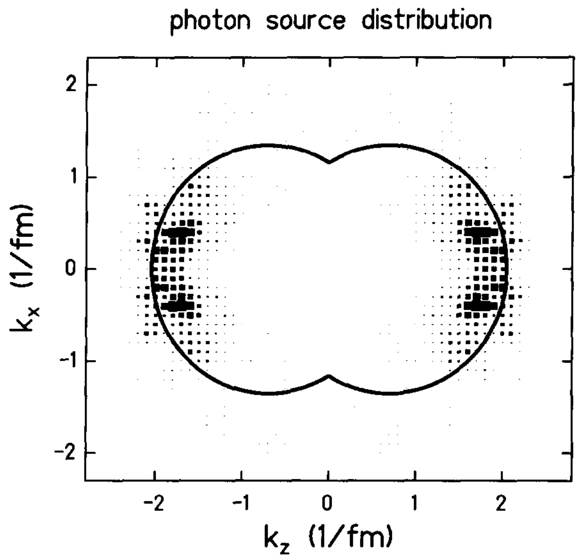

Fig. 10. The distribution of nucleons $R(\boldsymbol{k})$ (5.2) in momentum space which produce a 100 MeV photon at 90° in a central collision of $^{12}C+{}^{12}C$ at 40 MeV/u. The momentum distribution corresponding to the infinite nuclear matter limit is given in terms of the shifted Fermi spheres.

The second question addresses the fate of nucleons after producing a 100 MeV γ-ray. Due to energy and momentum conservation the region with $k_z \approx 0$ is favored, but it is Pauli-forbidden in the infinite nuclear matter limit. To see the actual population of this region we show the probability that the phase-space around k_3 is vacant:

$$P(\boldsymbol{k}_3)=\sum_i [1-f(\boldsymbol{r}_i; \boldsymbol{k}_3; t_i)] \tag{5.3}$$

in fig. 11. Here we have summed over all pn collisions i that produce a 100 MeV photon at 90° (for $^{12}C+^{12}C$ at 40 MeV/u). $\boldsymbol{k}_3$ and $\boldsymbol{k}_4$ are constrained by momentum and energy conservation while the remaining relative angle Ω is chosen randomly and then averaged out. The shifted Fermi spheres corresponding to the infinite nuclear matter limit are also displayed in fig. 11 for ease of comparison.

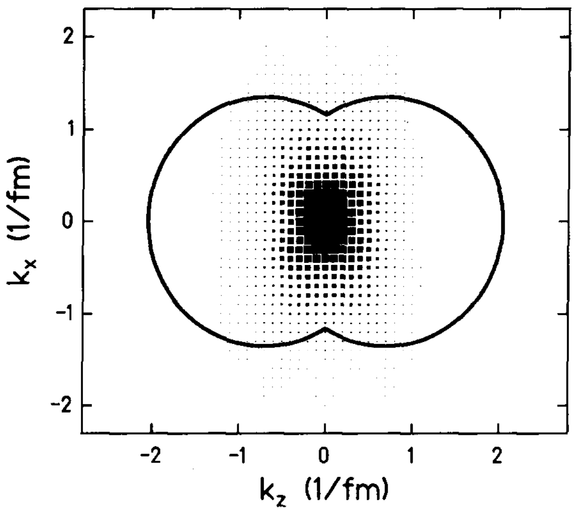

Fig. 11. The final phase-space probability $P(\boldsymbol{k})$ (5.3) for final states of nucleons producing a 100 MeV photon at 90° in a mutual collision for $^{12}C+^{12}C$ at 40 MeV/u.

We find that the $k_z \approx 0$ region is indeed strongly favored. That there is any free phase-space in this region in contrast to the infinite nuclear matter limit can be traced back to distortions in phase space for finite colliding nuclei which keep the low momentum region around $k_z \approx 0$ unoccupied [18,19,36,37]). Nucleon–nucleon collisions start to fill up this part of phase space within roughly 10 to 15 fm/c [ref. [36])] so that this effect again limits the production of energetic γ-rays to the early phase of the heavy-ion collision.

We now analyze the apparent source velocity of high energy photons in the laboratory frame. Since in our present approach the photons arise from individual pn collisions the source velocity of each photon is given by that of the c.m. of the respective pn system. By summing over all collisions i we can define a source velocity distribution by

$$N(\boldsymbol{v}) = \sum_i W_i[\boldsymbol{k}_1, \boldsymbol{k}_2; \boldsymbol{k}_\gamma]\delta[\boldsymbol{v} - \hbar(\boldsymbol{k}_1(i) + \boldsymbol{k}_2(i))/2M], \tag{5.4}$$

where we use a nonrelativistic notation since relativistic corrections turn out to be negligible for this study.

The numerical result for $N(v_z)$ integrated over the perpendicular velocity components is shown in fig. 12 (full line) where we have summed over all pn collisions i which produce a 50 MeV photon at $\theta = 90°$ for $^{12}C + ^{12}C$ at 40 MeV/u. The distribution $N(v_z)$ peaks at half beam velocity ($v/c \approx 0.144$). This result is not surprising since we deal with a symmetric system in which the nucleon-nucleon and the nucleus-nucleus c.m. velocities coincide.

Performing the same analysis for a central collision of $^{12}C + ^{40}Ca$ at 40 MeV/u we obtain the source velocity distribution $N(v_z)$ denoted in fig. 12 by the dashed line. If the photons were emitted in the compound nucleus rest frame we would expect $N(v_z)$ to be peaked around $v/c \approx 0.06$ which, however, is not at all the case

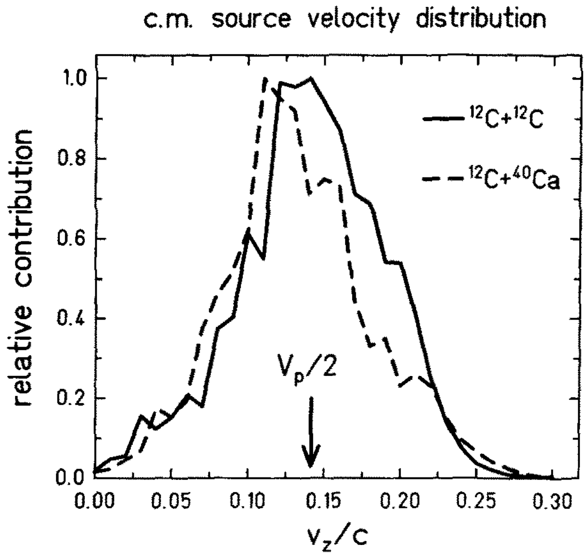

Fig. 12. The source velocity distribution $N(v_z)$ (5.4) for 50 MeV photons at 90° in case of central collisions of $^{12}C + ^{12}C$ (full line) and $^{12}C + ^{40}Ca$ (dashed line) at 40 MeV/u.

in accordance with experimental observation [1-8]). The distribution is only slightly shifted compared to the symmetric case $^{12}C + ^{12}C$ expressing the fact that energetic photon production is dominated by first chance pn collisions.

The source-velocities exhibit in both cases rather broad distributions which reflect the fact that also initial momenta contribute to the γ-production which are not opposite and equal in the midrapidity frame. In both cases treated the source velocity distributions are symmetrical within the statistics reflecting again the localization of the initial momenta to the pole-caps in momentum space.

6. Conclusion and outlook

We have performed a microscopic study of energetic photon production in proton and heavy-ion induced reactions based on a covariant model for bremsstrahlung from elementary proton–neutron collisions. Our detailed dynamical study allows the following conclusions:

(i) Energetic photon production is limited to the early stage of the reaction and dominated by first chance proton–neutron collisions.

(ii) Consequently the apparent source velocity is associated with the nucleon–nucleon frame of reference, i.e. the midrapidity domain.

(iii) Since proton–nucleus and nucleus–nucleus collisions are described on the same footing our simultaneous reproduction of both sets of experimental data leaves only minor room for coherent and cooperative reaction mechanisms*.

(iv) The high yield of photons observed must be attributed to distortions in phase-space which keep the midrapidity regime partly unblocked during the initial phase of the reaction (cf. fig. 11).

(v) Inclusive yields of energetic photons roughly scale with $(A_1 \cdot A_2)^{0.92}$.

In spite of the apparent success of the present theory one might worry about the limitations inherent in the classical phase-space approach. High momentum tails of the quantal wave-function might have a significant effect on very energetic photon yields as in case of pions [36]). A direct comparison of the results from the quantal first collision model [18]) and the classical BUU approach [19]) for $^{40}Ar+^{40}Ca$ at the low energy of 20 MeV/u, however, shows that for photon energies from 50 to 100 MeV we obtain an enhancement by quantal corrections of the order of 15% only [8]).

Since energetic photons are found to originate from the nonequilibrium stage of a nucleus–nucleus collision and since they suffer only negligible reabsorption due to the weak electromagnetic interaction, they can be used as triggers for more exclusive experiments which are expected to complete our understanding of non-equilibrium dynamics of finite fermion systems.

The authors acknowledge valuable and stimulating discussions with G.F. Bertsch, A. Gobbi, P. Grimm, E. Grosse, N. Herrmann, R. Hingmann, V. Metag and H. Nifenecker during the course of this study.

References

1) E. Grosse, P. Grimm, H. Heckwolf, W.F.J. Müller, H. Noll, A. Oskarsson and H. Stelzer, Europhys. Lett. **2** (1986) 9
2) N. Herrmann, J. Albinski, R. Bock, E.P. Feng, R. Freifelder, A. Gobbi, P. Grimm, E. Grosse, K.D. Hildenbrand, H.T. Liu, W.F.J. Müller, H. Stelzer, P. Braun-Munzinger, J. Stachel, P.R. Maurenzig, A. Olmi and A.A. Sefanini, Gesellschaft für Schwerionenforschung Annual Report 1985, p. 86
3) J. Stevenson, K.B. Beard, W. Benenson, J. Clayton, E. Kasky, A. Lampis, D.J. Morrissey, M. Samuel, R.J. Smith, C.L. Tam and J.S. Winfield, Phys. Rev. Lett. **57** (1986) 555

* This statement is so far substantiated only for collisions with relatively "light" heavy ions. Since collective processes scale with Z^2 compared to Z for the incoherent production, collective bremsstrahlung might dominate in reactions between the heaviest nuclei (cf., however, the discussion in sect. 4.3).

4) M. Kwato Njock, M. Maurel, E. Monnand, H. Nifenecker, J. Pinston, F. Schussler and D. Barneoud, Phys. Lett. **175B** (1986) 125;
R. Bertholet, M. Kwato Njock, M. Maurel, E. Monnand, H. Nifenecker, P. Perrin, J.A. Pinston, F. Schussler, D. Barneoud, C. Guet and Y. Schutz, Nucl. Phys. A, submitted
5) K. Beard, W. Benenson, C. Bloch, E. Kasky, J. Stevenson, D.J. Morissey, J. van der Plicht, B. Sherril and J.S. Winfield, Phys. Rev. **C32** (1986) 1111
6) N. Alamanos, P. Braun-Munzinger, R.F. Freifelder, P. Paul, J. Stachel, T.C. Awes, R.L. Ferguson, F.E. Obenshain, F. Plasil and G.R. Young, Phys. Lett. **173B** (1986) 392
7) R. Hingmann, W. Kühn, V. Metag, R. Mühlhans, R. Novotny, A. Ruckelshausen, W. Cassing, H. Emling, R. Kulessa, H.J. Wollersheim, B. Haas, J.P. Vivien, A. Boullay, H. Delagrange, H. Doubre, C. Gregoire and Y. Schutz, Phys. Rev. Lett. **58** (1987) 759
8) P. Grimm, PhD thesis, GSI report 87-2
9) D. Vasak, W. Greiner, B. Müller, T. Stahl and M. Uhlig, Nucl. Phys. **A428** (1984) 291c;
D. Vasak, B. Müller and W. Greiner; J. of Phys. **C11** (1985) 1309
10) D. Vasak, Phys. Lett. **176B** (1986) 276
11) T. Stahl, M. Uhlig, B. Müller, W. Greiner and D. Vasak, preprint GSI 86-46
12) W. Bauer, W. Cassing, U. Mosel, M. Tohyama and R.Y. Cusson, Nucl. Phys. **A456** (1986) 159
13) K. Nakayama and G.F. Bertsch, Phys. Rev. **C34** (1986) 2190
14) R. Shyam and J. Knoll, Nucl. Phys. **A448** (1986) 322
15) J. Knoll, J. de Phys. **C4** (1986) 185
16) H. Nifenecker and J.P. Bondorf, Nucl. Phys. **A442** (1985) 478
17) C.M. Ko, G.F. Bertsch and J. Aichelin, Phys. Rev. **C31** (1985) 2324
18) W. Cassing, T. Biro, U. Mosel, M. Tohyama and W. Bauer, Phys. Lett. **181B** (1986) 217
19) W. Bauer, G.F. Bertsch, W. Cassing and U. Mosel, Phys. Rev. **C34** (1986) 2127
20) G.F. Bertsch, H. Kruse and S. Das Gupta, Phys. Rev. **C29** (1984) 673
21) H. Kruse, B. Jacak and H. Stöcker, Phys. Rev. Lett. **54** (1985) 289;
H. Kruse, B. Jacak, J.J. Molitoris, G.D. Westfall and H. Stöcker, Phys. Rev. **C31** (1985) 1770
22) J. Aichelin and G.F. Bertsch, Phys. Rev. **C31** (1985) 1730
23) D. Neuhauser and S.E. Koonin, Nucl. Phys. **A462** (1987) 163
24) J.D. Jackson, Classical electrodynamics (Wiley, New York, 1962) ch. 15
25) R. Baier, H. Kühnelt and P. Urban, Nucl. Phys. **B11** (1969) 675
26) G.E. Bohannon, L. Heller and R.H. Thompson, Phys. Rev. **C16** (1977) 284
27) V.R. Brown and J. Franklin, Phys. Rev. **C8** (1973) 1706
28) P.F.M. Koehler, K.W. Rothe and E.H. Thorndike, Phys. Rev. Lett. **18** (1967) 933
29) J.D. Walecka, Ann. of Phys. **83** (1974) 491
30) T.S. Biro, J. Zimanyi and M. Zimanyi, Phys. Lett. **167B** (1986) 271
31) K. Chen, Z. Fraenkel, G. Friedlaender, J.R. Grover, J.M. Miller and Y. Shimamoto, Phys. Rev. **166** (1968) 949
32) G.F. Bertsch, J. Borisowicz and H. McManus, Nucl. Phys. **A284** (1977) 399
33) C. Itzykson and J.-B. Zuber, Quantum field theory (McGraw-Hill, 1985) p. 697
34) J. Cugnon, T. Mizutani and J. Vandermeulen, Nucl. Phys. **A352** (1981) 505
35) J.A. Edgington and B. Rose, Nucl. Phys. **89** (1966) 523
36) W. Cassing, Phase space approach to nuclear dynamics, ed. M. Di Toro (World Scientific, Singapore 1986) pp. 64-93
37) M. Tohyama, R. Kaps, D. Masak and U. Mosel, Proc. Workshop on nuclear dynamics III, Copper Mountain 1984, Indiana Univ. report INC-40007-24, p. 165